Effects of ultrasound irradiations time over Ni–Mo/γ-Al₂O₃ catalyst synthesis for 1,3 – Propanediol selectively via aqueous phase reforming of glycerol

Francis Wang Sing Yu, Mariam Ameen, Aqsha Aqsha, Mohammad Izham, Mohammad Tazli Azizan, and Farooq Sher

Effects of ultrasound irradiations time over Ni–Mo/γ-Al₂O₃ catalyst synthesis for 1,3 – Propanediol selectively via aqueous phase reforming of glycerol

Francis Wang Sing Yu [a,b], Mariam Ameen [a,b,*], Aqsha Aqsha [c,**], Mohammad Izham [a,b], Mohammad Tazli Azizan [d], Farooq Sher [e]

[a] HiCoE, Center for Biofuels and Biochemical Research (CBBR), Institute of Sustainable Building (ISB), Malaysia
[b] Department of Chemical Engineering, Universiti Teknologi PETRONAS, Bandar Seri Iskandar, 32610, Perak, Malaysia
[c] Department of Bioenergy and Chemurgy EngineeringFaculty of Technology IndustryInstitut Teknologi Bandung, Indonesia
[d] Faculty of Chemical Engineering Technology, University Malaysia Perlis, Kompleks Pusat Pengajian Jejawi 3, 02600, Arau, Perlis, Malaysia
[e] School of Mechanical, Aerospace and Automotive Engineering, Faculty of Engineering, Environmental and Computing, Coventry University, Coventry, CV1 5FB, UK

ABSTRACT

In general, aqueous phase reforming (APR) is used to convert glycerol into 1,3-propanediol (1,3-PDO), nonetheless, studies have shown a low selectivity of 1,3-PDO. Therefore, this study aims to optimize the selectivity of 1,3-PDO by varying the ultrasound (Us) irradiation process time between 10 and 50 min during catalyst preparation. This is to investigate the effect on the physiochemical properties and activity of the catalyst. Ni–Mo/Al₂O₃ catalysts were prepared using a sonochemical method and was characterized using Brunauer-Emmett-Teller (BET), X-ray Powder Diffractometer (XRD), Field Emission Scanning Electron Microscopy (FESEM) and Hydrogen Temperature-programmed Reduction (H₂-TPR). Characterization results revealed that there were significant improvements in physiochemical properties of catalysts by varying the Ultrasound (Us) irradiation time. Subsequently, all catalysts were screened using APR of glycerol for 1,3-PDO production using an Autoclave PREMEX reactor and the liquid products were analyzed to determine the selectivity of 1,3-PDO. From all the results, findings revealed that the catalyst prepared with 10 min of Us radiation time demonstrated a high catalytic performance and physiochemical properties while producing the highest concentration of 1,3-PDO with 954 ppm with a conversion of 38.6%. The outcomes have shown that sonochemical irradiation time conversely effects on the physiochemical properties of the catalysts and 1,3-PDO production.

1. Introduction

In general, biomass has shown low impact towards the environment even though carbon dioxide is produced as a by-product during combustion. This is because the carbon dioxide emitted during the combustion reaction will be recycled by trees and plants to absorb it for photosynthesis process. Several types of thermochemical processes have been used to convert biomass such as lignocellulose materials into value-added chemicals and fuel energy.

Aqueous phase reforming (APR) is one of the most promising and well-developed techniques to produce hydrogen and liquid valuable products such as 1,3-propanediol, acetone and methanol. 1,3-propanediol (1,3-PDO) is amongst the most expensive chemical and economical compound which is generally produced by the hydration of acrolein which is also an expensive route for production. The market size of 1,3-PDO is estimated to reach $490 million by the end of 2019 and is projected to reach $870 million by 2024 [1]. Recent researches have shown that APR is also a promising thermochemical process for 1,3-PDO production using glycerol as a raw product over the most suitable catalyst. This is to utilize the oversupply of glycerol by converting into a value-added product as it was reported that the supply of glycerol was approximately 8.4 billion pounds and the market of glycerol evolved mainly due to the increase in biodiesel manufacturing process in 2018 [2]. Nevertheless, the development to selectively produce 1,

3-propanediol from glycerol is not an easy path as studies in recent years shows that the main products produced from glycerol through APR are mainly 1,2-propanediol and propanols which doesn't have significant importance in industries. Substantial amount of 1,3-propanediol can only be produced when oxide of group VI or VII is added as a promoter to increase the selectivity of 1,3-propanediol. Therefore, the research is still ongoing to find the most suitable catalyst for a high selectivity of 1,3-PDO via APR process using renewable resources. This is because there are several possibilities that the preparation method of catalyst and the type of catalyst used favor the production of 1,3-PDO. Based on previous research, Nickel (Ni) based catalyst was found to be suitable for APR process as it helps to promote the formation of C–C bond cleavage during the reaction [3]. By using a metal catalyst, a promoter was reported to be required to stabilize the catalyst at higher temperatures and prevent coking which would deactivate the catalyst [4,5]. Thus, adding small amount of Molybdenum (Mo) was found to increase catalytic performance of Nickel (Ni) based catalyst and promote the production of 1, 3-propanediol. Besides, a catalyst support is commonly used with metal catalyst to enhance the performance of the catalyst by increasing the surface area [6] and aluminum oxide (Al_2O_3) is used to support Ni catalyst. Therefore, Ni–Mo/Al_2O_3 was identified as the catalyst for APR process to convert glycerol to 1,3-PDO.

There are several methods in preparing catalyst, however the sonochemical method was discovered to be the most suitable method to synthesize catalyst as it uses the presence of high frequency ultrasonic waves and it does not require any usage of complicated facilities to carry out the preparation [7]. In addition, sonochemical method will increase the dispersion of metal particles on the support system and alter the morphology of the precursors which will prevent agglomeration while increasing the surface area for reaction to occur [8]. Nevertheless, it was reported that sonochemical method has shown better physiochemical properties of catalyst in terms of morphology structure and surface area when compared to other conventional methods [9]. Hence, sonochemical method was the selected preparation process for the catalyst to increase the selectivity towards the desired product which is 1,3-PDO via APR of glycerol. It was carried out by determining the effect of ultrasound irradiation time on the physiochemical properties of the catalyst as it was reported by previous research that the irradiation time will affect the size of metal particles which directly affects the dispersion and crystallinity structure of the catalyst [8]. Thus, the project aims to identify the best ultrasound irradiation process time for the catalyst synthesis to achieve the highest selectivity and yield of 1,3-PDO via APR of glycerol.

2. Methodology

2.1. Materials

Materials that were used to synthesize the catalyst are as follows: Nickle (II) Nitrate Hexahydrate (Ni(NO$_3$)$_2$·6H$_2$O) as the Nickel promoter, Ammonium Heptamolybdate Tetrahydrate ((NH$_4$)$_6$Mo$_7$O$_{24}$·4H$_2$O) as Molybdenum precursor and Aluminum Oxide (γ-Al_2O_3) as the catalyst support. The chemicals were purchased from Sigma-Aldrich Malaysia Sdn Bhd with its respective purity of Nickle (II) Nitrate Hexahydrate (>98.5%), Ammonium Heptamolybdate Tetrahydrate (>99.0%) and Aluminum Oxide (>99.99%).

2.2. Catalyst synthesis

All the catalysts were prepared via sonochemical method where ultrasonic (Us) irradiation was introduced during the preparation. The weight percentage of metal loading for nickel (Ni), molybdenum (Mo) and aluminum oxide (Al_2O_3) were 10 wt%, 5 wt% and 85 wt% respectively and this metal loading percentage was chosen based on previous investigation. By using the determined weight percentage of metal loading and the molecular weight of each compound, the amount of Ni(NO$_3$)$_2$·6H$_2$O and (NH$_4$)$_6$Mo$_7$O$_{24}$·4H$_2$O were 4.945 g and 6.44 g,

respectively. Fig. 1 shows the procedure in preparing the bimetallic solid Ni–Mo/γ-Al_2O_3 catalyst. The preparation of catalysts began by mixing the Ni(NO$_3$)$_2$·6H$_2$O and (NH$_4$)$_6$Mo$_7$O$_{24}$·4H$_2$O in 25 mL of deionized water individually and each solution was put in the sonicator for 30 s at 90 Watt before mixing both solution onto the γ-Al_2O_3 support. The mixture was put in the sonicator to apply ultrasonic irradiation for 10–50 min at 90 Watt with a 30 s pulse ON and 15 s pulse OFF. The sonicator used for this preparation was Q700 Sonica Sonicator. After sonication, the samples were dried for approximately 12 h in an oven at 110 °C before calcinating at 550 °C for 4 h. The sonication process time for the catalysts preparation were varied from 20, 30, 40, and 50 min to study the effect of sonication time towards the catalyst. The sonication time is actual process time of interaction of sonication probe and catalysts material excluding pulse OFF.

2.3. Catalyst characterization

All catalysts were subjected to characterization to investigate the physiochemical properties of the bimetallic catalyst. The characterization techniques used to study the properties of the catalysts were X-Ray Diffraction (XRD), Brunauer-Emmett-Teller (BET), Field Emission Scanning Electron Microscopy (FESEM) and Temperature-Programmed Reduction (H$_2$-TPR).

XRD was used to determine the unit cell dimensions and to identify the crystalline phase structure of the catalyst. The samples were analyzed using a Cu Kα radiation source and the scan of range for the analyses were taken to be $10° < 2θ < 90°$ on the XRD analyzer (Bruker AXS D8 Advance). The crystalline size of particles was calculated using Scherer formula as shown in Equation (1) where the D = Size of Crystallite (nm), K = Crystallite Shape Factor = 0.94, θ = Angle of Peak (radian), λ = Constant = 1.54 nm and β = Width at Maximum Intensity of Peak (radian).

$$D = \frac{K\lambda}{\beta \cos\theta} \qquad (1)$$

BET analysis was used to specifically determine the surface area of the catalysts including the distribution of pore sizes and pore volume with illustration of the physical adsorption of gas particles on solid surface. The analysis was measured using an automatic volumetric adsorption unit (Micrometric ASAP 2020 Instrument Corp.) at liquid nitrogen temperature. All the analyses were analyzed using nitrogen multilayer adsorption and desorption isotherms through the ASAP2020V3·04H analyzer.
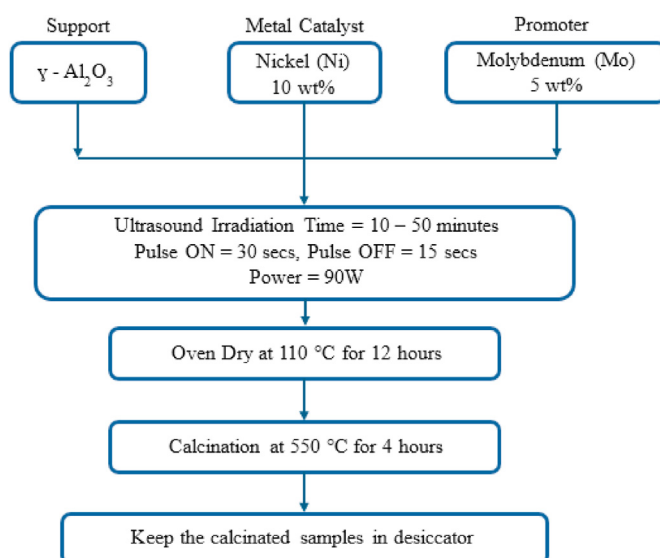
Fig. 1. Flow chart of catalyst synthesis.

FESEM techniques were carried out to determine the surface morphology of the catalyst using the VPFESEM, Zeiss Supra 55 VP with a high magnification of up to 10,000x and this provided an optimum image of the catalyst surface morphology as well as the dispersion of metal particles on the support surface. The technique was coupled with Electron Dispersion X-Ray (EDX) to identify the surface metal composition (wt.%) while the dot mapping analysis was coupled with FESEM to determine the surface homogenous dispersion of metal particles over the support. All the samples were placed on a carbon-coated disc and the internal camera was adjusted to attain the desired images.

H$_2$-TPR was used to identify the reduction temperature and degree of reducibility of the catalyst using hydrogen gas. The characterization was performed using TPDRO1100, Thermo scientific and a U-shaped quartz reactor was utilized to place the samples to perform the test. The reactor was heated from 300 to 900 °C with the rate of 5 °C/min while introducing H$_2$ with a flow rate of 50 mL/min.

2.4. Catalyst activity test

The catalysts were firstly reduced using hydrogen gas (H$_2$), followed by the aqueous phase reforming reaction using a Parr reactor with glycerol. 10 wt% (25 mL) of glycerol solution was prepared in 250 mL of distilled water as the feed for APR reaction. Besides, the activation of the catalyst was performed using a fixed bed vertical tubular reactor where approximately 2 g of catalyst was used and loaded into the reactor tube while using quartz wool as the catalyst bed. Then, the reactor was heated up to 550 °C at a ramping of 10 °C/min. Once the set temperature was achieved, 50% of hydrogen gas and nitrogen gas were introduced into the reactor at a flow rate of 30 mL/min, respectively for 1 h at 1 bar. The reduction procedure was repeated identically for all the catalysts.

Subsequently, for the performances of catalyst, aqueous phase reforming reaction was performed using PREMEX Autoclave reactor. 2 g of reduced catalyst was put into the reactor together with the glycerol solution. The reaction of APR was set at 230 °C and 20 bars while introducing nitrogen gas for 1 h with a rotational speed of 450 rpm. At the stated operating condition, it is sufficient for the APR process to produce liquid solution. After the experiment is completed, liquid product was collected for further analysis.

2.5. Product analysis

Liquid products were collected after the aqueous phase reforming reaction and the liquid product was analyzed using the High-Performance Liquid Chromatography (HPLC) to determine the quantitative amount of desired product which is 1,3-propanediol in liquid form. The detector used in the HPLC equipment for this project was the Refractive Index and the column used was Eclipse ZDB C18. The HPLC was operating at 30 °C and 40 bars while injecting the 0.005 M of Sulphuric Acid (H$_2$SO$_4$) as mobile phase. Qualitative results were attained from HPLC analysis as a series of peaks were observed from the results which represents glycerol and 1,3-propanediol. A calibration curve for pure glycerol and 1,3-propanediol was plotted. The calibration curve was used to determine the concentration of individual compounds by using the respective peak areas which was obtained from the HPLC analysis. Once the concentration of the desired compound was calculated, the conversion and selectivity of 1,3-propanediol can be computed using Equations (2) and (3).

$$Conversion \ (\%) = \frac{Glycerol \ Feed \ In - Glcyerol \ Feed \ Out}{Glycerol \ Feed \ In} \times 100\% \quad (2)$$

$$Selectivity \ (\%) = \frac{Amount \ of \ 1,3 - Propanediol}{Glycerol \ Feed \ In - Glycerol \ Feed \ Out} \times 100\% \quad (3)$$

3. Results and discussion

All synthesized catalysts were prepared with different ultrasonic irradiation time which varied from 10 to 50 min using the same composition of metal loading. Several labels were introduced throughout the experiment as shown in Table 1.

3.1. Catalyst characterization

The synthesized catalysts were characterized to investigate the effect of ultrasound irradiation time towards the physiochemical properties of the catalysts.

The XRD peak spectrum for γ-Al$_2$O$_3$ and 5 synthesized catalysts are illustrated in Fig. 2. Based on the XRD pattern, the γ-Al$_2$O$_3$ diffraction peaks were observed at an angle of 2θ = 37.50°, 47.50° and 67.80° (JCPDS-29-0063) which indicates the cubic structure of γ-Al$_2$O$_3$ [10]. The addition of nickel and molybdenum show an increment in the intensity of peak for the catalysts that indicates there is a good formation of crystalline structure. NiO peaks were detected at an angle of 2θ = 28.00°, 33.40° and 41.80° (JCPDS-078-6794) which shows the presence of NiO in the monoclinic structure [11]. The presence of NiO peak indicates that the Ni(NO)$_3$ was decomposed into NiO due to the calcination of the catalyst. In addition, Mo$_3$O peaks were found at an angle of 2θ = 14.5°, 23.70°, 32.36° and 44.29° which indicates that it is a cubic structure. Furthermore, it is observed that the peaks intensity of CAT 50 is lower than the intensity of CAT 10 as shown in Fig. 3. The Intensities gradually increased as shown in Fig. 3 (zoom in at peak around 28.00° at 2θ for NiO) for CAT10 to CAT50. The numbers for counts per second 255 (CAT10), 264 (CAT 20), 272 (CAT 30), 288 (CAT 40) and 306 (CAT50) represent the increase in intensities. This shows the clear difference in increase in intensities and crystallinity with increase if sonication time. However, the differences between the peak intensity shows slight insignificant and the intensity can be correlated with the FESEM analysis to determine the agglomeration of particles on the support surface and a further correlation on both analyses can be found in the following section. In addition, Table 2 demonstrates the crystallite size of particles in the catalyst which can be calculated using the Scherer correlation (Equation (1)). The crystalline size of the catalysts shows an increasing trend as the sonication time of catalyst increases. Lower crystallite size of particles indicates a higher specific surface area of catalyst [12]. The observation shown is correlated to the results from BET and FESEM analysis (see Fig. 4).

Besides, Fig. 4 shows the images of FESEM results for the catalyst at 10,000X magnification. From the results, the images demonstrated that the dispersion of metallic particles were homogeneously dispersed on the support as less agglomerated particles were observed. This is because ultrasound irradiation was proven to increase the dispersion of metal particles while synthesizing the catalysts [9]. The homogenous particle distribution is mainly due to the ultrasound irradiation which creates a phenomenon called cavitation. This phenomenon produces nanoscale bubbles that breaks down rapidly after being formed which causes the metal particles to be evenly distributed [13,14]. This observation from FESEM analysis is in line with the XRD results which also proves that the metal particles were homogeneously dispersed on the support. Furthermore, the figures of FESEM showed a trend for the dispersion of Nickel and Molybdenum particles on the support where the agglomeration of

Table 1
Description and label of synthesized catalyst.

Label	Description
CAT 10	● 10 min of ultrasonic irradiation
CAT 20	● 20 min of ultrasonic irradiation
CAT 30	● 30 min of ultrasonic irradiation
CAT 40	● 40 min of ultrasonic irradiation
CAT 50	● 50 min of ultrasonic irradiation
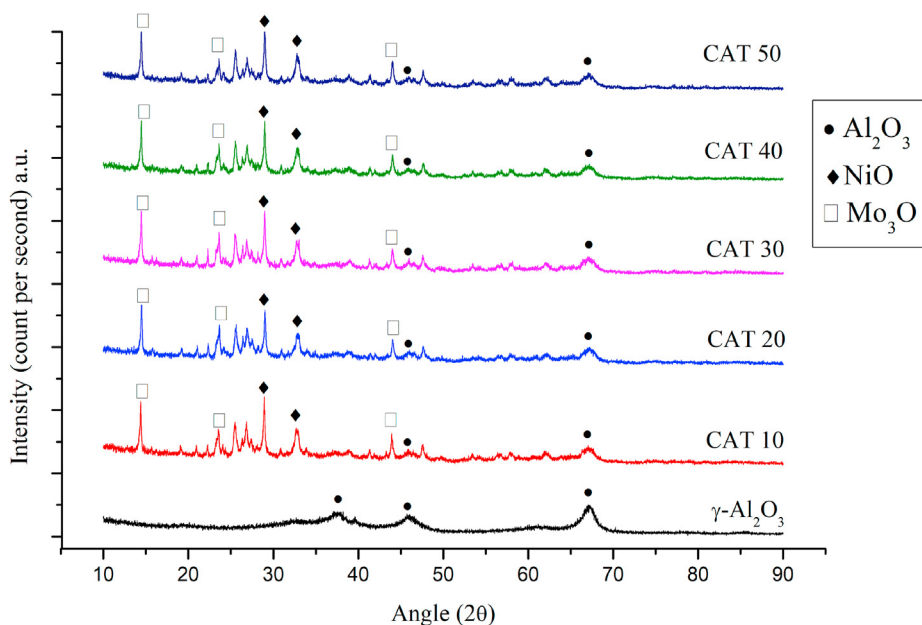
Fig. 2. XRD Pattern for all synthesized catalysts.
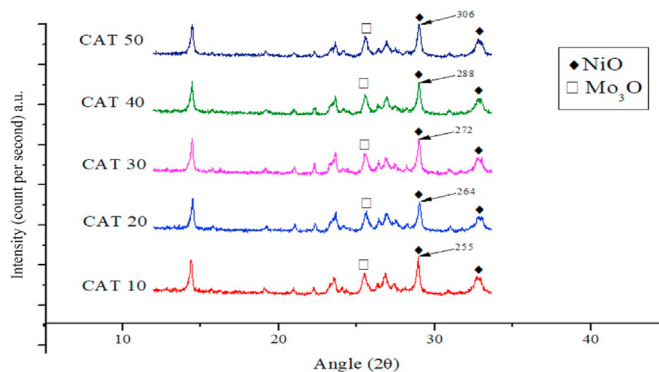
Fig. 3. Zoom in XRD Pattern for all the catalysts to highlight intensities in counts per second.

metal particles decreases as ultrasonic irradiation time increases. This is proven as the images of CAT 10 has lesser agglomeration of metal particles compared to CAT 50.

Generally, increasing sonication power contributes to more uniform dispersion on the surface morphology and smaller particle size [15,16]. Therefore, longer intense ultrasonic irradiations can limit the growth of metal particles and a more uniform morphology with additional highly dispersed particles were being observed. However, the results obtain through this project showed the opposite trend whereby increasing ultrasonic irradiation time caused an increase in agglomeration of metal particles. This phenomenon might be due to the properties of metal particles used in the catalyst. It was reported that properties of solid in liquid-solid mixture, especially its malleability, has an impact on the physiochemical properties of catalyst during the exposure of ultrasonic irradiation [17]. This is because acoustic cavitation-induced shock waves are introduced during ultrasonic irradiation and this may lead to various physical phenomena. Since nickel and molybdenum are classified as malleable materials, thus increasing ultrasonic irradiation will lead to agglomeration because of the collision between particles [18,19]. The velocity between colliding particles can be high during the impact between them and this may cause intense localized heating, plastic deformation and sintering to occur [20]. Consequently, increasing sonication time may produce a higher velocity of the particle and this may lead to

more rapid and vigorous collision between particles.

Meanwhile, the images of FESEM proves that there is a slight reduction of peak intensity from CAT 10 to CAT 50. This is because the increase in agglomeration as shown by the FESEM analyses causes the intensity of peak to decrease when sonication time increases. Decreasing crystallite size indicates an increase in peak intensity [21]. Sharper peaks which indicate higher peak intensity correlated to lesser agglomeration of metal particles. The reduction in intensity of main peaks suggests that the structure of the elements in the catalyst are changing from a high crystal form to an amorphous state [22].

On the other hand, BET analysis was performed to measure the specific surface area of catalysts which includes the pore size distribution, and this information is useful to estimate the dissolution rate of the catalyst. Table 3 shows the information of surface area, pore volume and pore size obtained from the analysis of all the catalyst. The data for surface area of catalyst was measured using BET method while pore volume and pore size was determined using Barrett-Joyner-Halenda (BJH) method. Based on the results shown, the surface area of the catalyst decreases with an increase in sonication time. Larger surface area will increase the area of contact between particles and this will result in more frequent successful collisions among reacting particles which will further increase the rate of reaction [23]. Nevertheless, the result indicated that at a higher sonication time, the agglomeration of metal particles is most likely to occur which causes the surface area of the support to be smaller [24]. Having agglomerated Ni and Mo particles may cause the pores of the support to be partially blocked, thus reducing the surface area for the support [25]. The surface area of CAT 10 to CAT 30 reduced consistently from 50.60 m^2/g to 45.50 m^2/g while there is sharp reduction in surface towards CAT40 and CAT50 where the surface area was 21.38 m^2/g and 18.01 m^2/g respectively. The large difference between CAT 30 and CAT 40 may be highly due to the increase in number of agglomerated particles on the surface between CAT 30 and CAT 40. As shown through the FESEM images, the agglomerated particles were seen to be more obvious on CAT 40 compared to CAT 30. Besides, the trend shown is in contrast with the general trend of sonication rate as it is mainly due to agglomeration over more sonication time Likewise, the pore size results indicate that the catalysts are categorized as mesoporous materials since all synthesized catalyst have a pore diameter between 2 and 50 nm [26,27]. Besides, the adsorption and desorption isotherm graph of all catalyst demonstrates the same curves which follows the
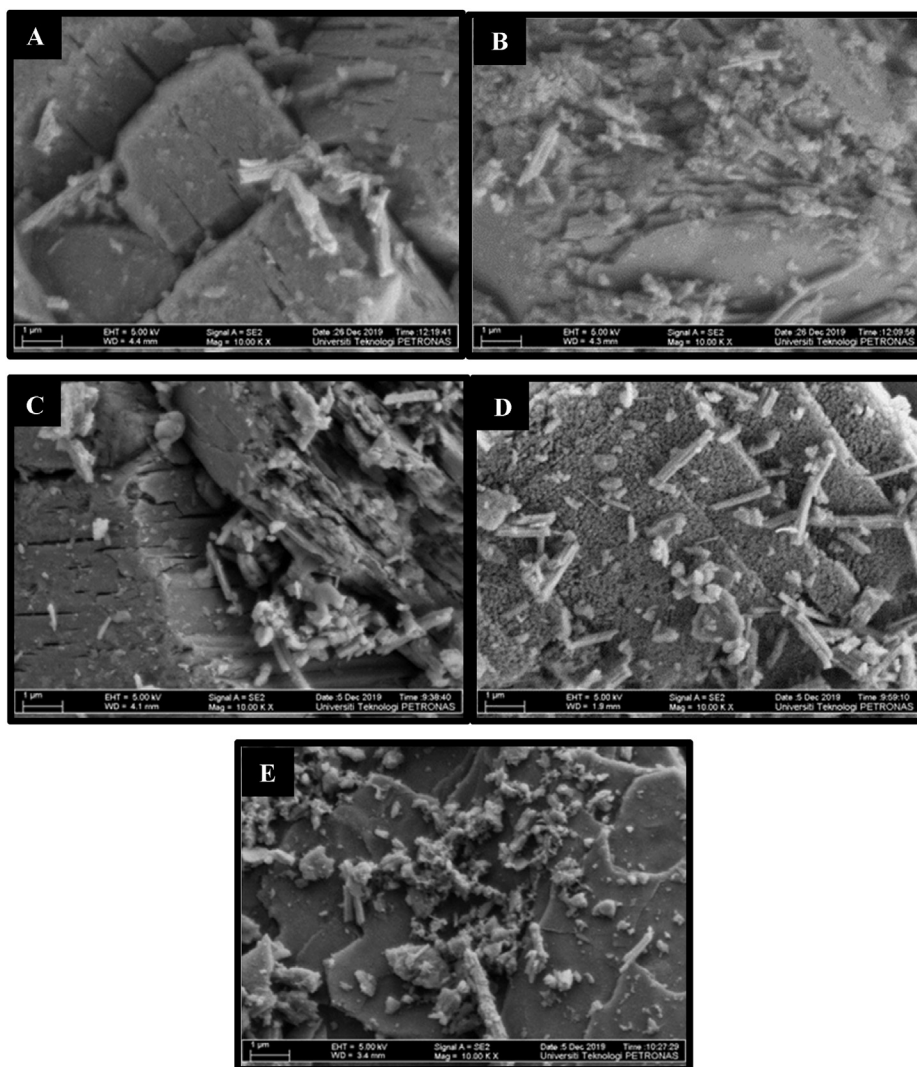
Fig. 4. Fesem images at 10000X magnification, (**A**) CAT 10**, (B)** CAT 20, (**C**) CAT 30, (**D**) CAT40, (**E)** CAT50.

Table 2
Crystallite size value of catalyst.

Catalyst Label	Crystallite Size (nm)
CAT 10	33.41
CAT 20	34.10
CAT 30	35.27
CAT 40	35.93
CAT 50	38.72

Table 3
Surface area, pore volume and pore size of catalyst.

Name	Sonication Time	Surface Area (m^2/g)	Pore Volume (cm^3/g)	Pore Size (nm)
CAT 10	10 min	50.60	0.13	5.58
CAT 20	20 min	49.79	0.11	5.31
CAT 30	30 min	45.50	0.10	5.52
CAT 40	40 min	21.38	0.05	5.53
CAT 50	50 min	18.01	0.04	5.62

Type IV isotherm.

Additionally, the H_2-TPR analysis is typically used to determine the optimum activation temperature of catalysts. Fig. 5 shows the graph of
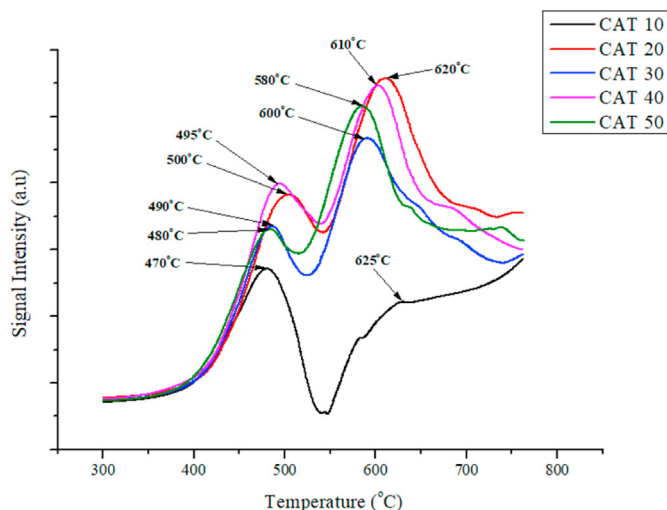
Fig. 5. H_2 - TPR Analysis of all the synthesized catalysts.

H_2-TPR analysis for all the catalyst and each peak represents the reduction temperature of a specific metal particles. According to the graph, two major peaks were clearly observed in the H_2 – TPR profiles of the catalysts. The first peak indicates the reduction temperature for nickel metal whereas the second peak correlates to the reduction temperature for molybdenum metal. The reduction profile of nickel metal has an upward trend as sonication time increases and the highest recorded reduction temperature is 505 °C. At the respective reduction temperature, nickel oxide (NiO) is being reduced to Ni [28]. The increasing trend of reduction temperature for Ni may be correlated to the dispersion of nickel metal particles on the support. This is because higher dispersion of particles will reduce the reduction temperature of the metals [29]. Furthermore, the second reduction peak that lies within the range of 580 °C–625 °C is attributed to the reduction of MoO_3 into MoO_2 [30]. There is no significant trend for the molybdenum metal which may be due to the inhomogeneous dispersion of molybdenum particles during sonochemical preparation and the reduction of catalyst which was carried out at 550 °C which is below the reduction temperature of molybdenum.

3.2. Product analysis

High Performance Liquid Chromatograph (HPLC) analysis was used to determine the concentration of 1,3-propanediol and the unconverted glycerol after APR. The concentration of 1,3-PDO and unconverted glycerol in the liquid products as well as the selectivity of 1,3-PDO and the conversion of glycerol were determined to compare the catalytic performance of the catalysts as shown in Table 4. From the results, it is observed that the concentration and selectivity of 1,3-PDO showed a decreasing trend with increase in sonication time. Besides, the conversion of glycerol also showed the similar trend whereby the conversion decreases as sonication time increases. Meanwhile, the unconverted glycerol illustrates a contrast trend in terms of concentration when the sonication time increases. From the result, CAT 10 was identified to be the best catalyst compared to other catalysts. This is because it contributed the highest concentration of 1,3-PDO with 954.5 ppm, the lowest concentration of unconverted glycerol with 73128.65 ppm and the highest selectivity of desired product with 2.08% with conversion of glycerol to be 38.57%. Since the selectivity of 1,3-PDO is only 2.08%, thus this indicates that there are other side products which are formed during this process.

The conversion of glycerol to 1,3-PDO largely depends on the active sites that are present on the catalyst surface. Therefore, when more active sites are formed, it increases the surface area due to the less agglomerated particles and this may lead to the increase in catalytic activity during the reaction [31,32]. An increase in agglomeration may block the active sites of metal particles to allow the reaction to take place on the surface [33]. Consequently, with an increase in catalytic activity, this may improve the production of 1,3-PDO. This proves that CAT 10 shows the highest performance among the catalyst as it has the largest surface area and the least agglomeration based on the characterization and product analysis. Therefore, to enhance the selectivity of 1,3-PDO via sonochemical method, catalysts with 10 min radiation time will be more effective compared to higher process time. Secondly, Ni–Mo/γ-Al_2O_3 is a commercial catalyst generally used for hydrogen production and from this preliminary investigation it is proved that 1,3-PDO can be achieved through APR process even with low selectivity. This selectivity can be enhanced by modification in catalysts design and synthesis route.

4. Conclusion

This study aims to investigate the effect of ultrasonic irradiation time to determine the effect towards the catalytic activity through the production of 1,3 -PDO from glycerol via APR. From the findings, it can be concluded that increasing the irradiation time on catalyst during sonochemical preparation method influences the physiochemical properties and the performance of catalyst. It is found that increasing the irradiation

Table 4
Product analysis over all the synthesized catalyst.

Name	Concentration (ppm)		Selectivity (%)	Conversion (%)
	Unconverted Glycerol	1,3 - Propanediol		
CAT 10	73128.65	954.53	2.08	38.57
CAT 20	76683.23	781.66	1.85	35.59
CAT 30	80288.28	666.31	1.72	32.56
CAT 40	81069.38	626.09	1.65	31.90
CAT 50	82724.09	590.40	1.63	30.51

time increases the agglomeration on the surface which may be due to the increase in induced-shock waves when the sonication time was increased. In addition, the specific surface of the catalyst shows a reduction when increasing the exposure time towards the ultrasound irradiation. Similarly, the crystallite size which is correlated to the surface area shows the opposite trend and this is because surface area is inversely proportional to the crystallite size. Furthermore, the reduction temperature shows an upward trend from CAT 10 to CAT 50 which indicates that lower the agglomeration on the surface would lead to lower reduction temperature. Besides, CAT 10 obtained the highest concentration of 1,3-PDO with 954.5 ppm and produces the lowest concentration of unconverted glycerol with 73128.65 ppm compared to other catalyst. From the findings, it proves that the catalyst with 10 min of sonication has the best catalytic performance as it demonstrates better physiochemical properties and higher selectivity of 1,3-PDO compared to the catalyst which was exposed for 50 min of ultrasound irradiation. Since the catalyst requires only 10 min of sonication time with a power of 90 W, thus this requires lesser consumption of energy during the preparation of catalyst. This shows that sonochemical method is more economically feasible compared to other conventional methods such as wet impregnation or co-precipitation. On the other hand, varying the ultrasound power was reported to provide an effect towards the catalyst properties. Thus, it is recommended to perform at a suitable ultrasound power to further enhance the efficiency of the catalyst.

Declaration of competing interest

The authors declare that they have no known competing financial interests or personal relationships that could have appeared to influence the work reported in this paper.

Acknowledgement

References

[1] Markets and Markets, 1,3-Propanediol (PDO) Market by Application - Global Forecast to 2024, Markets and Markets, 2019.

[2] C.A.G. Quispe, C.J.R. Coronado, J.A. Carvalho Jr., Glycerol: production, consumption, prices, characterization and new trends in combustion, Renew. Sustain. Energy Rev. 27 (2013) 475–493.

[3] Y. Guo, X. Liu, M.U. Azmat, W. Xu, J. Ren, Y. Wang, G. Lu, Hydrogen production by aqueous-phase reforming of glycerol over Ni-B catalysts, Int. J. Hydrogen Energy 37 (1) (2012) 227–234.

[4] S. Katheria, A. Gupta, G. Deo, D. Kunzru, Effect of calcination temperature on stability and activity of Ni/MgAl2O4 catalyst for steam reforming of methane at high pressure condition, Int. J. Hydrogen Energy 41 (32) (2016) 14123–14132.

[5] J. Kugai, V. Subramani, C. Song, M.H. Engelhard, Y.H. Chin, Effects of nanocrystalline CeO2 supports on the properties and performance of Ni–Rh bimetallic catalyst for oxidative steam reforming of ethanol, J. Catal. 238 (2) (2006) 430–440.

[6] S.S. Maluf, E.M. Assaf, Ni catalysts with Mo promoter for methane steam reforming, Fuel 88 (9) (2009) 1547–1553.

[7] M. Abdollahifar, M. Haghighi, A.A. Babaluo, Syngas production via dry reforming of methane over Ni/Al2O3–MgO nanocatalyst synthesized using ultrasound energy, J. Ind. Eng. Chem. 20 (4) (2014) 1845–1851.

[8] M.R. Vaezi, S.M. Kazemzadeh, A. Hassanjani, A. Kazemzadeh, Effects of ultrasound irradiation time on the synthesis of lead oxide nanoparticles by sonochemical method, J. Optoelectron. Adv. Mater. 17 (9–10) (2015) 1458–1463.

[9] M. Ameen, M.T. Azizan, A. Ramli, S. Yusup, M.S. Alnarabiji, Catalytic hydrodeoxygenation of rubber seed oil over sonochemically synthesized Ni-Mo/γ-Al2O3 catalyst for green diesel production, Ultrason. Sonochem. 51 (2019) 90–102.

[10] M. El-Kemary, N. Nagy, I. El-Mehasseb, Nickel oxide nanoparticles: synthesis and spectral studies of interactions with glucose, Mater. Sci. Semicond. Process. 16 (6) (2013) 1747–1752.

[11] S.K.W. Ningsih, M. Khair, Synthesis and characterization of nio nanocrystals by using sol-gel method with various precursors, Makara Journal of Science 21 (1) (2017) 4.

[12] K. Raj, B. Viswanathan, Effect of surface area, pore volume and particle size of P25 titania on the phase transformation of anatase to rutile, Indian J. Chem. 48A (2009) 1378–1382.

[13] M. Abdollahifar, M. Haghighi, A.A. Babaluo, Syngas production via dry reforming of methane over Ni/Al2O3–MgO nanocatalyst synthesized using ultrasound energy, J. Ind. Eng. Chem. 20 (4) (2014) 1845–1851.

[14] N. Ahmadi, K. Germaschewski, J. Raeder, Effects of electron temperature anisotropy on proton mirror instability evolution, J. Geophys. Res.: Space Physics 121 (6) (2016) 5350–5365.

[15] A. Abedini, A.R. Daud, M.A.A. Hamid, N.K. Othman, E. Saion, A review on radiation-induced nucleation and growth of colloidal metallic nanoparticles, Nanoscale Research Letters 8 (1) (2013) 1–10.

[16] S. Mahboob, M. Haghighi, F. Rahmani, Sonochemically preparation and characterization of bimetallic Ni-Co/Al2O3-ZrO2 nanocatalyst: effects of ultrasound irradiation time and power on catalytic properties and activity in dry reforming of CH4, Ultrason. Sonochem. 38 (2017) 38–49.

[17] L. Hiremath, Nipun, Sruti, Kala, Aishwarya, Sonochemistry: Applications in Biotechnology, Sonochemical Reactions. Selcan Karakuş, IntechOpen, 2018, https://doi.org/10.5772/intechopen.88973.

[18] K.S. Suslick, G.J. Price, Applications of ultrasound to materials chemistry, Annu. Rev. Mater. Sci. 29 (1) (1999) 295–326.

[19] S.J. Doktycz, K.S. Suslick, Interparticle collisions driven by ultrasound, Science 247 (4946) (1990) 1067–1069.

[20] H.N. Kim, K.S. Suslick, The effects of ultrasound on crystals: sonocrystallization and sonofragmentation, Crystals 8 (7) (2018) 280.

[21] N. Li, G.W. Huber, Aqueous-phase hydrodeoxygenation of sorbitol with Pt/SiO2–Al2O3: identification of reaction intermediates, J. Catal. 270 (1) (2010) 48–59.

[22] E.M. Abdelrazek, A.M. Abdelghany, S.I. Badr, M.A. Morsi, Structural, optical, morphological and thermal properties of PEO/PVP blend containing different concentrations of biosynthesized Au nanoparticles, Journal of materials research and technology 7 (4) (2018) 419–431.

[23] S. Sun, H. Li, Z.J. Xu, Impact of surface area in evaluation of catalyst activity, Joule 2 (6) (2018) 1024–1027.

[24] S. Pradhan, J. Hedberg, E. Blomberg, S. Wold, I.O. Wallinder, Effect of sonication on particle dispersion, administered dose and metal release of non-functionalized, non-inert metal nanoparticles, J. Nanoparticle Res. 18 (9) (2016) 1–14.

[25] M. Lv, W. Xie, S. Sun, G. Wu, L. Zheng, S. Chu, J. Bao, Activated-carbon-supported K–Co–Mo catalysts for synthesis of higher alcohols from syngas, Catalysis Science & Technology 5 (5) (2015) 2925–2934.

[26] M. Tahir, N.S. Amin, Photocatalytic CO2 reduction and kinetic study over In/TiO2 nanoparticles supported microchannel monolith photoreactor, Appl. Catal. Gen. 467 (2013) 483–496.

[27] J. Dang, G.H. Zhang, K.C. Chou, R.G. Reddy, Y. He, Y. Sun, Kinetics and mechanism of hydrogen reduction of MoO3 to MoO2, Int. J. Refract. Metals Hard Mater. 41 (2013) 216–223.

[28] K.V. Manukyan, A.G. Avetisyan, C.E. Shuck, H.A. Chatilyan, S. Rouvimov, S.L. Kharatyan, A.S. Mukasyan, Nickel oxide reduction by hydrogen: kinetics and structural transformations, J. Phys. Chem. C 119 (28) (2015) 16131–16138.

[29] A. Arevalo-Bastante, M. Martin-Martinez, M.A. Álvarez-Montero, J.J. Rodriguez, L.M. Gómez-Sainero, Properties of carbon-supported precious metals catalysts under reductive treatment and their influence in the hydrodechlorination of dichloromethane, Catalysts 8 (12) (2018) 664.

[30] J. Dang, G.H. Zhang, K.C. Chou, R.G. Reddy, Y. He, Y. Sun, Kinetics and mechanism of hydrogen reduction of MoO3 to MoO2, Int. J. Refract. Metals Hard Mater. 41 (2013) 216–223.

[31] A. Ciftci, B. Peng, A. Jentys, J.A. Lercher, E.J. Hensen, Support effects in the aqueous phase reforming of glycerol over supported platinum catalysts, Appl. Catal. Gen. 431 (2012) 113–119.

[32] D.A. Boga, F. Liu, P.C. Bruijnincx, B.M. Weckhuysen, Aqueous-phase reforming of crude glycerol: effect of impurities on hydrogen production, Catalysis Science & Technology 6 (1) (2016) 134–143.

[33] S. Bagheri, N. Muhd Julkapli, S. Bee Abd Hamid, Titanium dioxide as a catalyst support in heterogeneous catalysis, Hindawi, The Scientific World Journal 2014 (2014), https://doi.org/10.1155/2014/727496.